4A.5 THE DETECTION OF LOW-LEVEL MISOVORTICES EMBEDDED WITHIN A QUASI-LINEAR CONVECTIVE SYSTEM ON 2 APRIL 2010 BY A CASA RADAR

Vivek N. Mahale[1,2] and J. Brotzge[1] and H. B. Bluestein[2]

[1]*Center for Analysis and Prediction of Storms, University of Oklahoma*
[2]*School of Meteorology, University of Oklahoma*

1. INTRODUCTION

On 2 April 2010, a quasi-linear convective system associated with a cold front moved northeastward through central Oklahoma around sunrise. At least three distinct vortices were embedded within this convective system. Two out of three vortices caused damage; the most significant damage was associated with the second vortex where a mobile home was rolled over from the strong winds on the southern side of Rush Springs.

The quasi-linear convective system formed between 0600 and 0700 UTC across northwest Texas ahead of a cold front that had merged earlier with a dryline. This convective system moved northeastward at around 30 to 35 m s^{-1} into Oklahoma. As it moved northeastward, it expanded in size and increased in intensity. The convective system passed over Rush Springs at approximately 1100 UTC (Fig. 1).

The sounding closest in time and space to the Rush Springs storm was taken at Norman (KOUN), Oklahoma at 1200 UTC (Fig. 2). The winds on the sounding are not contaminated by convection since the winds behind the convection veered to the west and later to the northwest at the surface. Since the winds in this sounding are not contaminated by convection, it is a reasonable representation of the environment at the time of the storm's peak intensity because the storms were located at Norman at 1200 UTC. The sounding was nearly saturated from the surface up to 650 hPa, but was much drier from 650 hPa to about 400 hPa. Surface based convective available potential energy (CAPE) was ~450 J kg^{-1}, while mixed-layer CAPE (MLCAPE) was ~1300 J kg^{-1}.

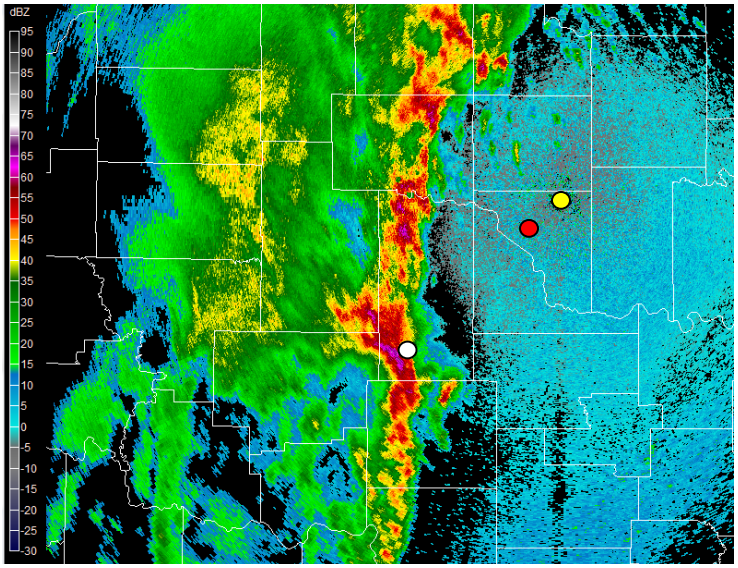

Fig. 1. KTLX NEXRAD base reflectivity at 1102 UTC. Data collected at 0.5° elevation angle. White circle indicates the location of Rush Springs. Yellow circle indicates the location of KTLX. Rush Springs is about 87 km to the southwest of KTLX. Red circle indicates the location of Norman, Oklahoma.

Corresponding author address: Vivek Mahale
School of Meteorology, 120 David L. Boren Blvd.
Suite 5900 Norman, Oklahoma 73072
Email: vmahale@ou.edu

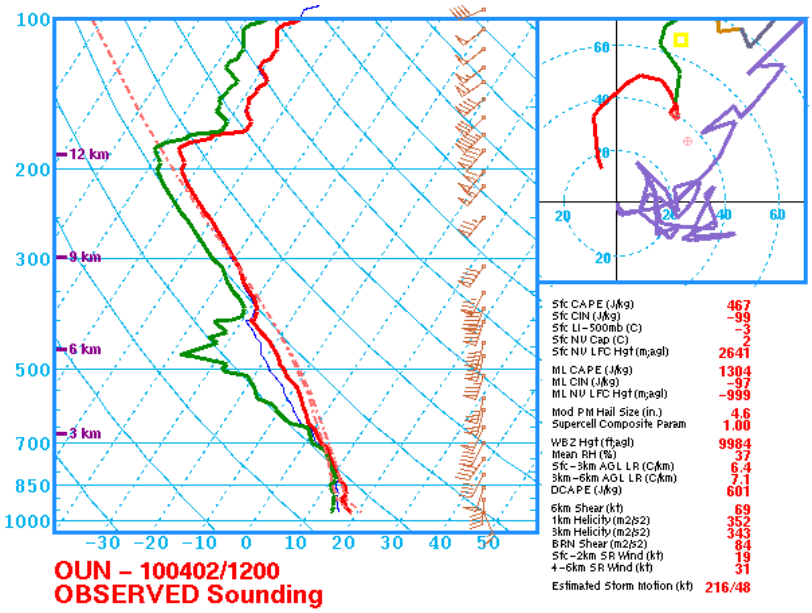

Fig. 2. KOUN sounding and hodograph from 1200 UTC. Note the presence of high directional wind shear in the lowest 1 km (red line on the hodograph). Sounding plot courtesy the Storm Prediction Center.

The sounding and hodograph indicate an environment characterized by a large amount of directional and speed wind shear, especially in the lowest km. This large amount of shear is represented on the hodograph as a large amount of curvature from the surface up to 1 km. There is also an outward push in the lowest km that can be attributed to the stronger winds associated with the LLJ.

The 0-1 km and 0-3 km helicity was ~350 m^2 s^{-2} and 0-6 km shear was ~35 m s^{-1}. Supercells that can produce tornadoes tend to be found in environments where 0-3 km storm relative helicity is at least 150 m^2 s^{-2} (Davies-Jones et al. 1990). Supercells also tend to be found in environments where 0-6 km shear is at least 20 m s^{-1} (Bluestein and Parker 1993). The estimated storm motion from the hodograph was ~215 degrees at nearly 25 m s^{-1}.

The purpose of this research is to document the evolution of the vortices beginning when the initial complex formed and continuing until the storm passed through Rush Springs.

2. THE CASA NETWORK

Approximately 25% of tornadoes are not warned by the National Weather Service (Brotzge and Erickson 2009), and around 75% of tornado warnings are false alarms (National Weather Service 2007). In addition, the ratio of tornadoes that are warned to those that are not warned decreases with distance from radar. There are several reasons why tornadoes have been so difficult to warn in advance: poor sampling in time and at low-levels, distance from radar, and lack of verification (Brotzge and Erickson 2010). One technological solution to these problems is being tested by the Engineering Research Center for the Collaborative Adaptive Sensing of the Atmosphere (CASA; McLaughlin et al. 2009) funded by the National Science Foundation.

CASA deployed a test bed of four X-band, dual-polarimetric radars in southwestern Oklahoma in fall 2006 as shown in Figure 3. Each radar has a beam width of 1.8°, oversamples every 1°, and has a range of about 40 km. The CASA network has overlapping radar coverage to provide dual-Doppler capability and to provide multiple radar views that can overcome radar attenuation (Chandrasekar and Lim 2008).

The vortices associated with the 2 April 2010 case were sampled best by the CASA radar near Rush Springs (KRSP). Thus, analysis will be conducted primarily through the use of that radar. NEXRAD radar data will also be used in the

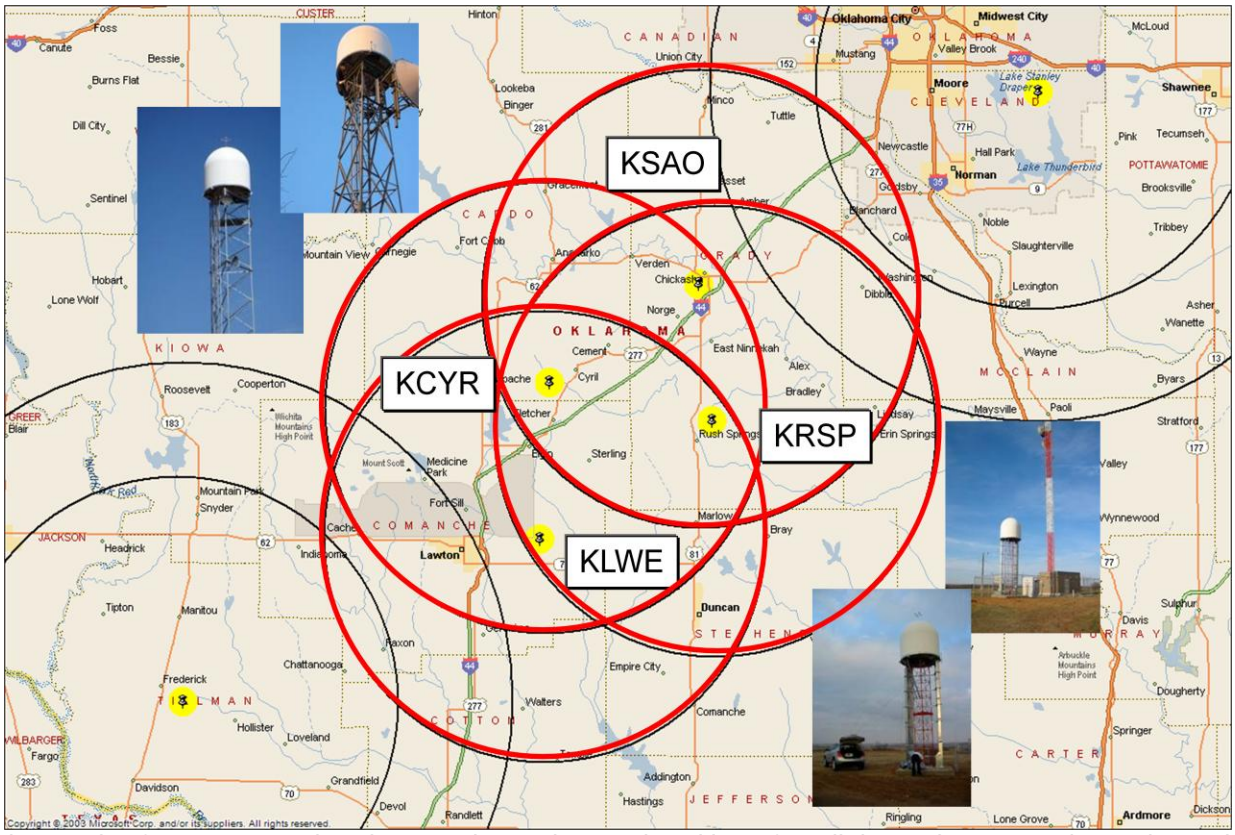

Fig. 3. The four CASA radar sites are located near the cities of Cyril (KCYR), Lawton (KLWE), Rush Springs (KRSP), and Chickasha (KSAO). Range rings of 40 km are shown in red around each CASA radar. The nearest NEXRAD radars are KTLX and KFDR; range rings of 40 km and 60 km are shown.

analysis to gain an understanding of the convective structure at higher levels.

3. ANALYSIS

Three low-level vortices were documented by the KRSP at 1.0° elevation angle. The first vortex entered the southwest edge of KRSP at 1044 UTC (not shown).

An area of higher differential reflectivity (Z_{DR}) was located to the northeast of this vortex. This zone of higher Z_{DR} resembles the polarimetric signature referred to as a "Z_{DR} arc" (Kumjian and Ryzhkov 2008). Z_{DR} arcs occur due to size sorting in which larger drops which have a higher terminal velocity are not advected as far as smaller drops because they fall out sooner; there is higher Z_{DR} in lower levels across the forward flank downdraft (FFD). Z_{DR} arcs have been previously documented by an X-band radar (Snyder et al. 2010). The first vortex and its associated Z_{DR} arc continued until approximately 1056 UTC. No damage was reported with this vortex.

A new vortex developed to the north of the first vortex around 16 km to the southwest of the radar at approximately 1055 UTC (Fig. 4). This vortex was the strongest of the three vortices with a max isodop to min isodop difference of just above 45 m s^{-1} at 1100 UTC. The strongest measured winds by KRSP were on the right side of the vortex because the storm motion was rapidly to the northeast. Some winds to the left of the vortex (with respect to its motion) were close to 0 m s^{-1} at times as a result of the fast motion. A well-defined hook can be seen with this vortex on reflectivity (Z_H). In addition, a Z_{DR} arc was associated with this vortex.

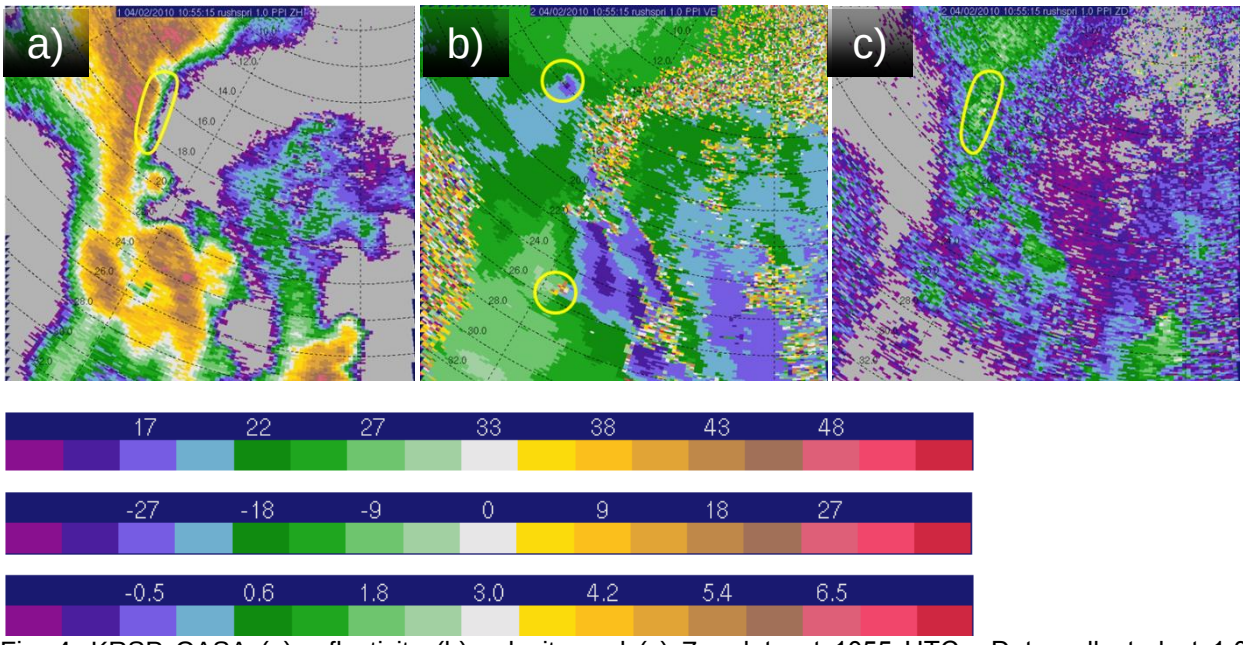

Fig. 4. KRSP CASA (a) reflectivity (b) velocity and (c) Z_{DR} data at 1055 UTC. Data collected at 1.0° elevation angle. The two vortices are highlighted by the yellow circles on the velocity. The region of the Z_{DR} arc is outlined in yellow on the reflectivity and Z_{DR} panels. Below the three panels, the color scales for reflectivity (dBZ), velocity (m s^{-1}) and Z_{DR} (dBZ) are shown.

The Z_{DR} arc from this vortex appears to have originated from the first vortex as large droplets were caught in the developing vortex. This vortex caused the most significant damage in Rush Springs.

A third vortex began to develop to the north of the second vortex at 1059 UTC (Fig. 5). As the vortex intensified between 1059 UTC and 1103 UTC, a Z_{DR} arc became established to the north of the third vortex. At the same time, the second vortex lost its association with a Z_{DR} arc (Fig. 6). The biggest jump with the Z_{DR} arc can be seen between 1102 UTC and 1103 UTC. It appears that the arc associated with the second vortex jumped to the north and became associated with the third vortex. At this time, the reflectivity associated with the second vortex depicts the precipitation in a closed loop. This vortex caused minor damage to the north of Rush Springs. At 1104 UTC, two distinct hooks can be seen within 4 km of KRSP (Fig. 7). It is difficult to deduce what happens to these vortices beyond 1105 UTC because the complex moved over KRSP, which attenuated the radar signal after that time.

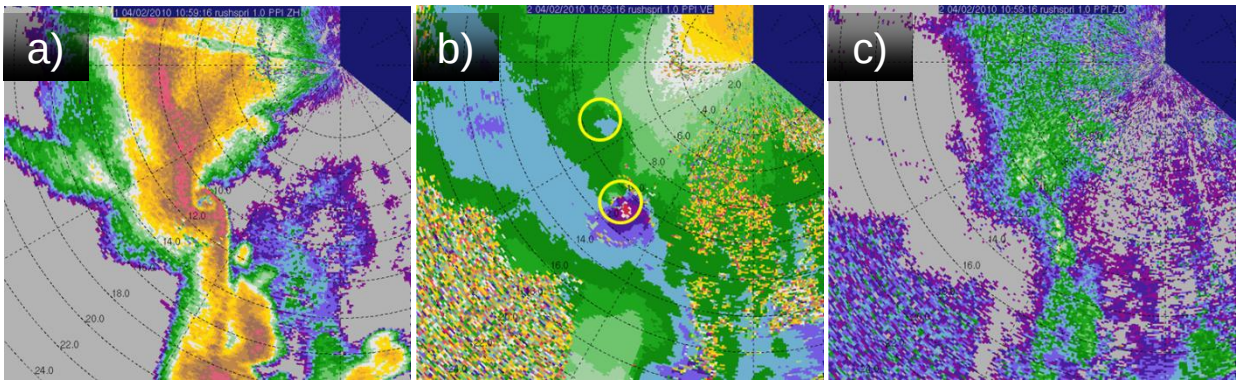

Fig. 5. KRSP CASA (a) reflectivity (b) velocity and (c) Z_{DR} data at 1059 UTC. Data collected at 1.0° elevation angle. The two vortices are highlighted by the yellow circles on the velocity panel. See Fig. 4 for the color scales.

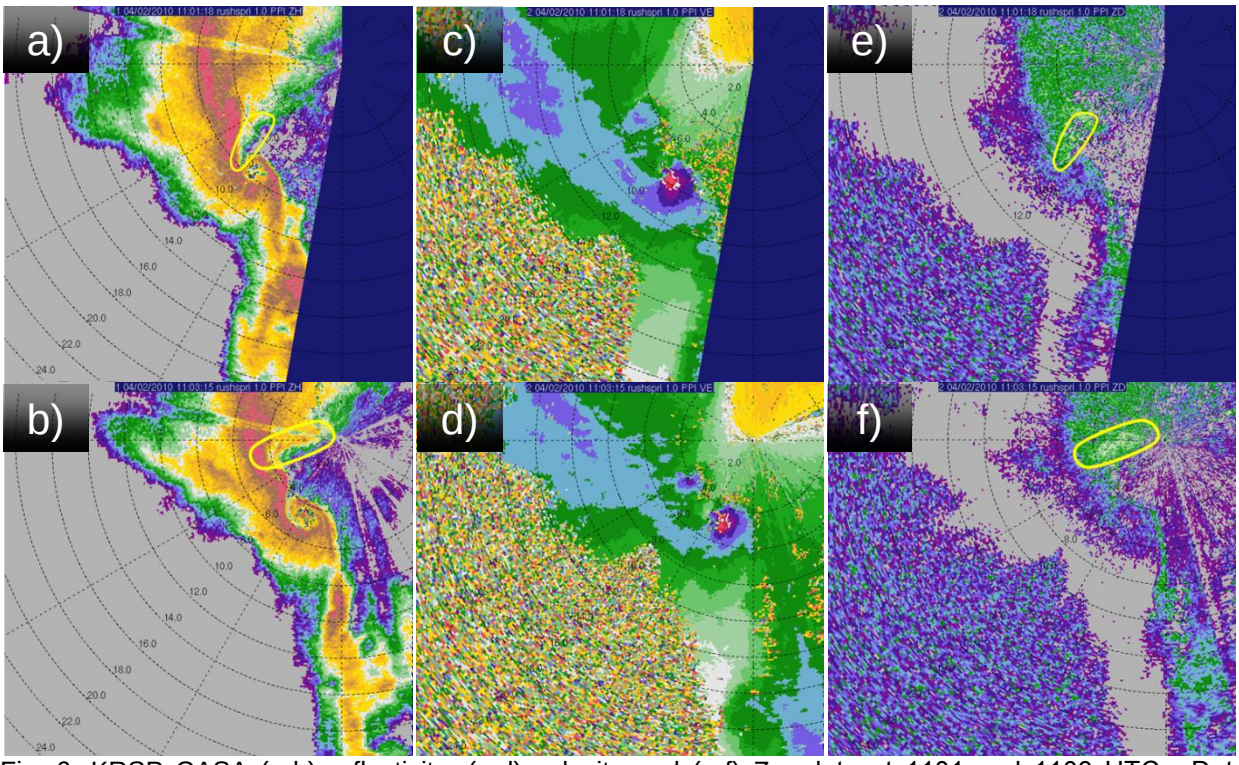

Fig. 6. KRSP CASA (a-b) reflectivity, (c-d) velocity and (e-f) Z_{DR} data at 1101 and 1103 UTC. Data collected at 1.0° elevation angle. The region of the Z_{DR} arc is outlined in yellow on the reflectivity and Z_{DR} panels. See Fig. 4 for the color scales.

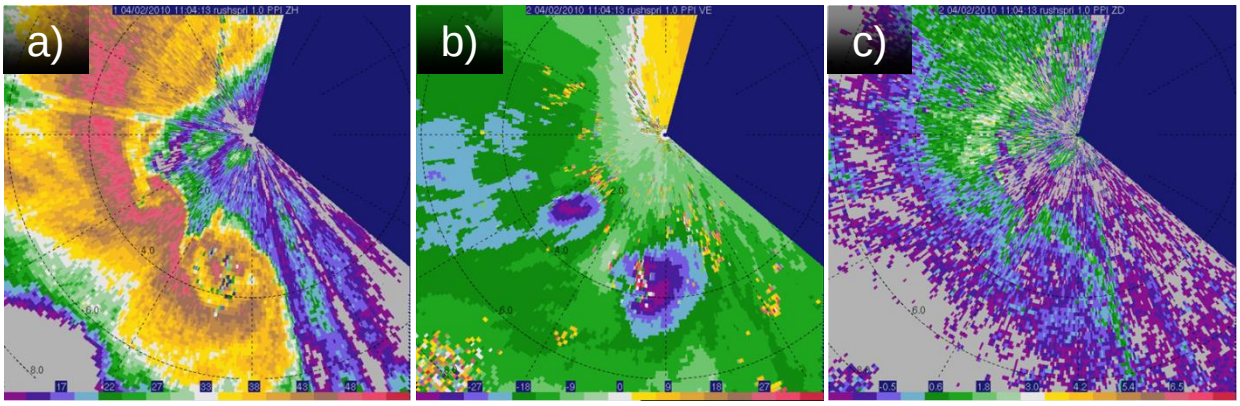

Fig. 7. KRSP CASA (a) reflectivity (b) velocity and (c) Z_{DR} data at 1104 UTC. Data collected at 1.0° elevation angle. See Fig. 4 for the color scales.

KTLX NEXRAD was able to see only one of the three vortices. At 0.5° elevation angle, KTLX scans approximately 1200 m above ground level (AGL) at Rush Springs. Thus, the radar is measuring the mesocyclone aloft associated with the surface vortex. The mesocyclone lasted approximately 30 minutes on KTLX (Fig. 9). The updraft associated with the mesocyclone and the surface vortices was persistent on KTLX and lasted for over an hour (Fig. 8).

Two of the three vortices caused damage; the second vortex caused the most damage (Fig. 10). The most significant damage was across the southern side of Rush Springs. The damage path was unique because most of the damage was on the right side of the vortices due to the fast storm motion to the northeast at around 30 to 35 m s^{-1}. Damage ranged from broken tree branches to a rolled over mobile home. The rolled over mobile home occurred near the peak intensity of the vortex (Fig. 11).

4. DISCUSSION

The damage in Rush Springs was caused by winds associated with a translating misocyclone embedded within a quasi-linear convective complex. This convective complex does not fit a discrete connective storm type. Instead, it shows hybrid characteristics associated with both supercells and squall lines.

On a broad view, a line of nearly continuous convection is seen. This defines a squall line (AMS 2000). However, upon closer inspection, a mesocyclone with a continuous (with respect to time) updraft is seen. This mesocyclone persisted for around 30 minutes and its associated updraft persisting for over an hour. A mesocyclone with an updraft defines a supercell (AMS 2000). The enhanced damage potential because of the hybrid nature of the convection demonstrates the importance in forecasting the mode of convection in scenarios where more than one simultaneous mode is possible.

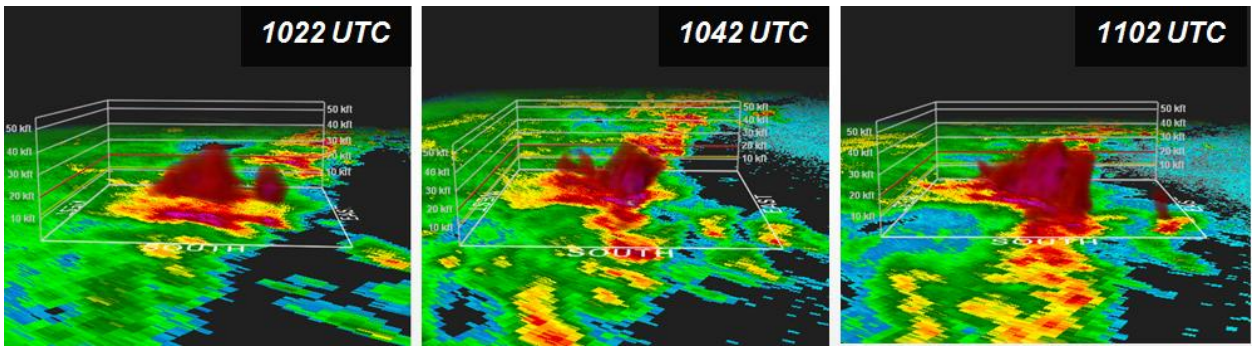

Fig. 8. KTLX NEXRAD reflectivity volume >50 dBZ at 20 minute increments of the same updraft.

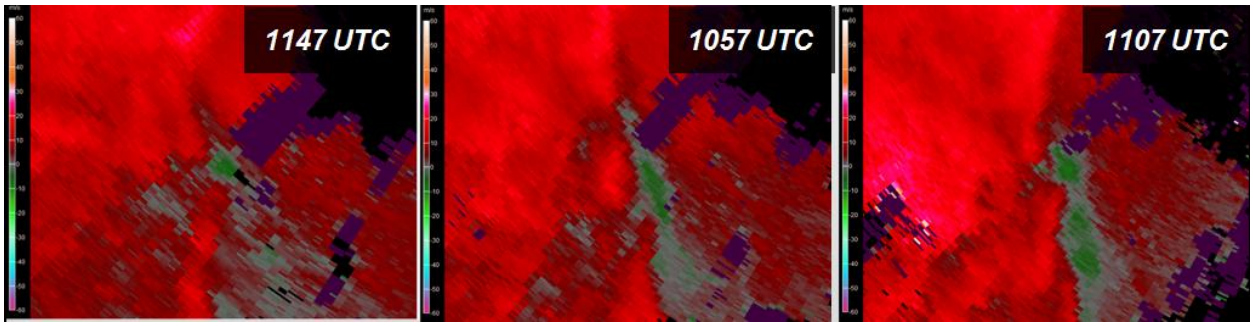

Fig. 9. KTLX NEXRAD storm relative velocity at 10 minute increments. Data collected at 0.5° elevation angle.

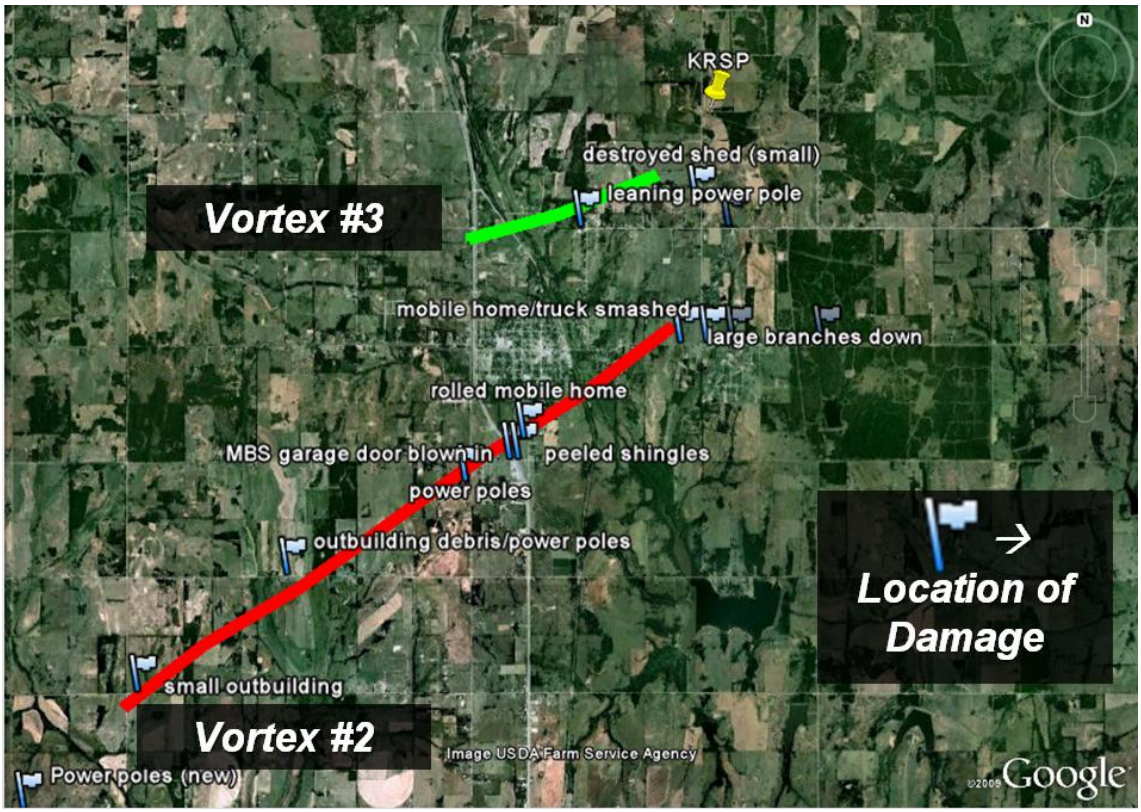

Fig. 10. Damage survey and path associated with the second and third vortices. Vortex paths were determined by KRSP CASA radar.

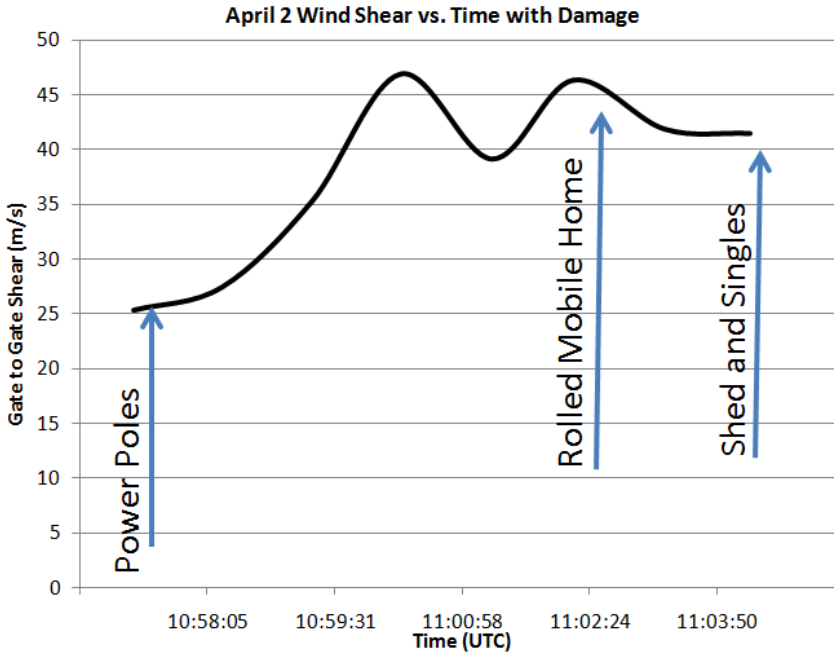

Fig. 11. Max isodop to min isodop difference at 1.0° elevation angle associated with the second vortex along with selected damage. Velocity measurements were difficult to discern beyond 1104 UTC because the storm approached the radar.

The fast storm motion makes it appear the damage is associated with straight line winds since the misocyclone's relative winds nearly cancel the storm motion to the left of the vortex and nearly double the ground-relative wind to the right of the vortex. However, it is apparent that when looking at the storm-relative winds, there is a vortex with max isodop to min isodop difference of just above 45 m s^{-1} at its peak. Essentially, the vortex decreased the damage potential on one the left side and increased damage potential on the right side of its center. Hence, detecting these small-scale vortices is important in making accurate warnings and forecasts during severe weather operations. Since these vortices were significantly easier to detect on a CASA radar than a NEXRAD radar, the benefits of having such a network present to fill in the gaps at low levels is apparent.

Overall, three vortices were detected by radar. All three vortices had a Z_{DR} arc at one time. It is interesting to note that the Z_{DR} arc seemed to be associated with the intensification of the vortex. In all three cases, the Z_{DR} arc became apparent as each vortex intensified. As a result, the movement of the Z_{DR} arc may have forecast implications in severe weather operations. Further studies will have to be done to assess the importance in the movement of the Z_{DR} arc as a predictive tool in severe convection.

Acknowledgments. The authors extend their appreciation to Jana Houser and Scott Hill for their assistance in converting the radar data among different formats. The authors also thank Kiel Ortega and Rachael Riley for conducting the damage survey. This work is supported by the Engineering Research Centers Program of the National Science Foundation under NSF Award 0313747. Any opinions, findings, conclusions, or recommendations expressed in this material are those of the authors and do not necessarily reflect those of the National Science Foundation.

References

AMS, cited 2010: Glossary of Meteorology. [Available online at http://amsglossary.allenpress.com/glossary].

Bluestein, H. B., and S. S. Parker, 1993: Modes of isolated, severe convective storm formation along the dryline. *Mon. Wea. Rev.,* **121**, 1354 – 1372.

Brotzge, J., and S. Erickson, 2009: NWS Tornado Warnings with Zero or Negative Lead Times. *Wea. Forecasting*, **24**, 140–154.

_____, and _____, 2010: Tornadoes with no NWS warning. *Wea. Forecasting*, **25**, 159-172.

Chandrasekar, V., and S. Lim, 2008: Retrieval of reflectivity in a networked radar environment. *J. Atmos. Oceanic Technol.*, **25**, 1755–1767.

Davies-Jones, R. P., D.W. Burgess, and M. Foster, 1990: Test of helicity as a forecast parameter. Preprints, *16th Conf. on Severe Local Storms*, Kananaskis Park, AB, Canada, AMS Conf., 588–592.

Kumjian, M. R., A. V. Ryzhkov, 2008: Polarimetric signatures in supercell thunderstorms. *J. of Appl. Met.,* **47**, 1940-1961.

McLaughlin, D., D. Pepyne, V. Chandrasekar, B. Philips, J. Kurose, et al., 2009: Short-wavelength technology and the potential for distributed networks of small radar systems. *Bull. Amer. Meteor. Soc.*, **90**, 1797-1817.

NWS, cited 2010: NOAA's NWS national performance measures FY 2006–FY National Weather Service. [Available online at http://www.nws.noaa.gov/com/files/All_GPRA2006.ppt.].

Snyder, J.C., H. B. Bluestein, G. Zhang, S. J Frasier, 2010: Attenuation Correction and Hydrometeor Classification of High-Resolution, X-band, Dual-Polarized Mobile Radar Measurements in Severe Convective Storms. *J. Atmos. Oceanic Technol.*, in press.